Inelastic analysis of RC beam-column subassemblages under various loading histories

Young-Chan You†

Building Structure & Production Division, Korea Institute of Construction Technology,
Taehwa-Dong, Ilsan-Gu, Koyang 411-410, Korea

Waon-Ho Yi‡

Department of Architectural Engineering, Kwang Woon University, Seoul 139-701, Korea

Li-Hyung Lee‡†

Department of Architectural Engineering, Han Yang University, Seoul 133-791, Korea

Abstract. The purpose of this study is to propose an analytical model for the simulation of the hysteretic behavior of RC (reinforced concrete) beam-column subassemblages under various loading histories. The discrete line element with inelastic rotational springs is adopted to model the different locations of the plastic hinging zone. The hysteresis model can be adopted for a dynamic two-dimensional inelastic analysis of RC frame structures. From the analysis of test results it is found that the stiffness deterioration caused by inelastic loading can be simulated with a function of basic pinching coefficients, ductility ratio and yield strength ratio of members. A new strength degradation coefficient is proposed to simulate the inelastic behavior of members as a function of the transverse steel spacing and section aspect ratio. The energy dissipation capacities calculated using the proposed model show a good agreement with test results within errors of 27%.

Key words: discrete line element; hysteretic model; inelastic rotational spring; plastic hinging zone; beam-column subassemblages; strength degradation; stiffness deterioration; energy dissipation capacity; cyclic loads; structural analysis.

1. Introduction

It is well known that a reinforced concrete frame building designed to resist code seismic forces will be stressed beyond the elastic limit during a major earthquake. When a ductile moment-resisting frame is subjected to large seismic lateral forces, the beam-to-column connection must be capable of carrying large moments and shear forces that are accompanied by relatively large

---

† Senior Researcher
‡ Associate Professor
‡† Professor

deformations. Recent advances have led to a better understanding of the design details necessary to assure satisfactory ductile behavior of such connections. However, it is essential that experimental studies keep pace with the development of analytical tools that can simulate the hysteretic behavior of structural members. Although the finite element method is generally considered to be a powerful analytical tool, its usefulness in design practice is limited because of the complex modeling problems of the various influence factors. Earlier efforts have shown that accurate analytical results can be obtained with relatively little effort (Otani 1974, Otani and Sozen 1972, Giberson 1967). Herein, a discrete line element model which is composed of elastic line elements with two inelastic rotational springs is proposed to simulate the hysteretic behavior of RC beams. The hysteretic rules are obtained from the analysis of laboratory test results.

2. Development of analytical model

2.1. Comparison of one-component discrete line element models

A member with plastic regions can be modeled as a nonprismatic beam containing finite size plastic regions at the ends, Fig. 1 (b). The length of a plastic region can be calculated assuming a linear distribution of moment along the member, Fig. 1 (a), (Arzoumanidis and Meyer 1981).

$$x_i = \frac{M_i - M_y}{M_i + M_j} L \tag{1}$$

Since the flexural rigidity varies irregularly within plastic regions due to the random occurrence of concrete cracks, its rigidity is assumed to be a weighted average of the plastic flexural rigidity at the column face and the elastic flexural rigidity, as proposed by Arzoumanidis and Meyer (1981),

$$\overline{EI} = \frac{(EI)_p \, (EI)_e}{c \, (EI)_e + (1-c) \, (EI)_p} \tag{2}$$

where the coefficient c varies between 0 and 1 and can be determined experimentally. The mean flexural rigidity of plastic hinging regions in such a one-component model is similar to the flexural rigidity of a plastic hinge in a one-component model with flexural rotational springs (Fig. 1 (c)) if $c=0.5$ is used, as shown in Appendix A. Moreover, an inconsistent choice of the coefficient c can lead to inaccurate results and an increase in computer run time because the mean flexural rigidity must be recalculated at each time step during a time history analysis. For this reason, the one-component flexural rotational spring model is adopted here, with which it is relatively easy to model the changing length of the plastic region.

2.2. Member modeling

The model of a beam-column consists of three parts: two rigid end zones, an elastic line element, and two rotational springs (Otani 1974, Al-Haddad and Wight 1986). The location of the rotational springs can be varied in accordance with the details of longitudinal reinforcement. The axial stiffness

$$K_{55} = K_{66} = -K_{56} = \frac{EA}{L} \tag{3}$$

is assumed to remain constant during inelastic response. The flexibility coefficients associated with rotational degrees of freedom can be obtained by the unit load method, Fig. 2, (Al-Haddad and Wight 1986):

$$F_{11} = f_{11} + f_{s1}(1 - x_p/L)^2 + f_{s2}(x_p/L)^2 \qquad (4)$$

$$F_{12} = f_{12} - (f_{s1} + f_{s2})(1 - x_p/L)(x_p/L) \qquad (5)$$

$$F_{21} = F_{12} \qquad (6)$$

$$F_{22} = F_{22} + f_{s1}(x_p/L)^2 + f_{s2}(1 - x_p/L)^2 \qquad (7)$$

where $f_{11} = f_{22} = L/3EI$, $f_{12} = f_{21} = -L/6EI$. f_{s1} and f_{s2} are the flexibilities of the rotational springs, and x_p is the length of the plastic region.

2.3. The primary moment-rotation curve

The moment-curvature relationships of plastic hinges are first evaluated at the critical sections, using three linear branches for monotonic loading: one for elastic loading, one for inelastic loading (strain hardening), and one for softening (Chung and Meyer 1989). For steel, the stress-strain curve of Brown and Jirsa (1971) and for concrete that of Mander, Priestley, and Park (1988) are adopted to determine the moment-curvature relationships of the plastic hinging zone. Assuming a linear distribution of moment along the member and an inflection point at midspan,
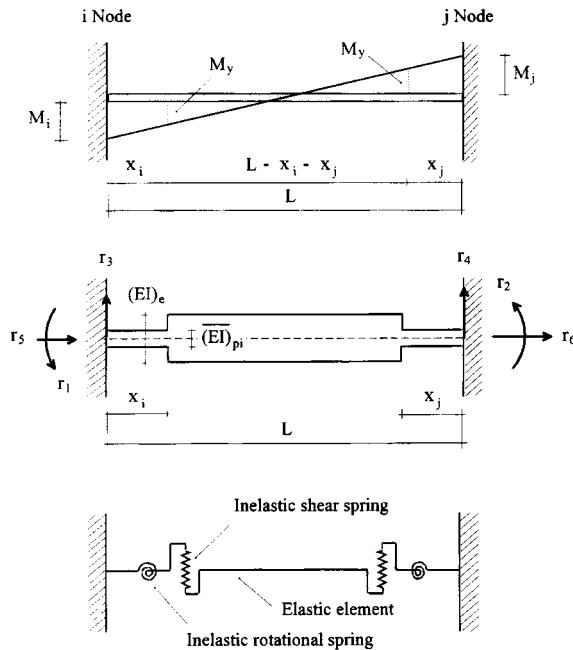
Fig. 1 (a) Moment diagram, (b) Modeling of discrete line element with finite plastic hinging zone, (c) Modeling of discrete line element with inelastic end springs
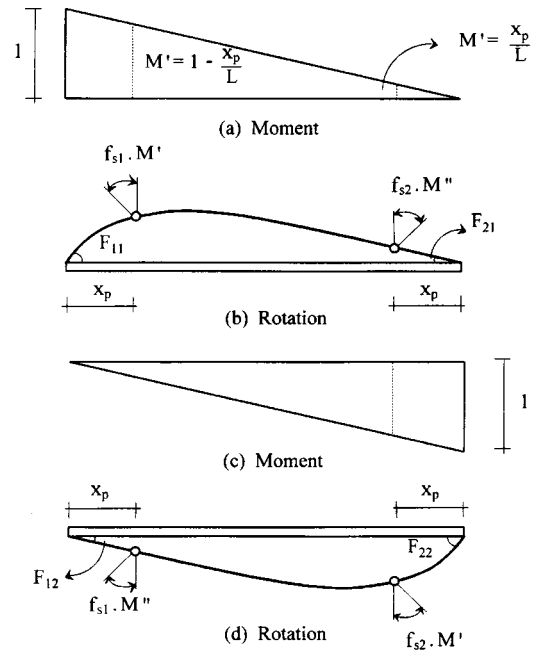
Fig. 2 Element rotation due to unit moment applied separately at each end

the member's primary moment-rotation relationship is obtained by integrating the curvatures over the plastic regions and the elastic portion of the beam.

3. Development of hysteresis rules

3.1. Basic hysteresis rules

The hysteresis rules are constructed by excluding variables that cannot be used in a dynamic analysis of an RC structure. They will be applicable in a two-dimensional inelastic frame analysis with six degrees of freedom per member. The proposed hysteresis function is composed of the six branches shown in Fig. 3.

1) Elastic Loading and Elastic Unloading: If the maximum moment does not exceed the yield moment M_y, the moment-rotation relationship is given by

$$\Delta M = K_1 \Delta\Theta = \frac{M_y}{\Theta_y} \Delta\Theta \tag{8}$$

where K_1 is the initial elastic member stiffness.

2) Inelastic Loading: If the moment exceeds the yield moment and is still increasing, the moment-rotation relationship is given by

$$\Delta M = K_2 \Delta\Theta = \frac{M_u - M_y}{\Theta_u - \Theta_y} \Delta\Theta \tag{9}$$

3) Inelastic Unloading: If the moment decreases after the yield moment has been exceeded, the moment-rotation relationship becomes
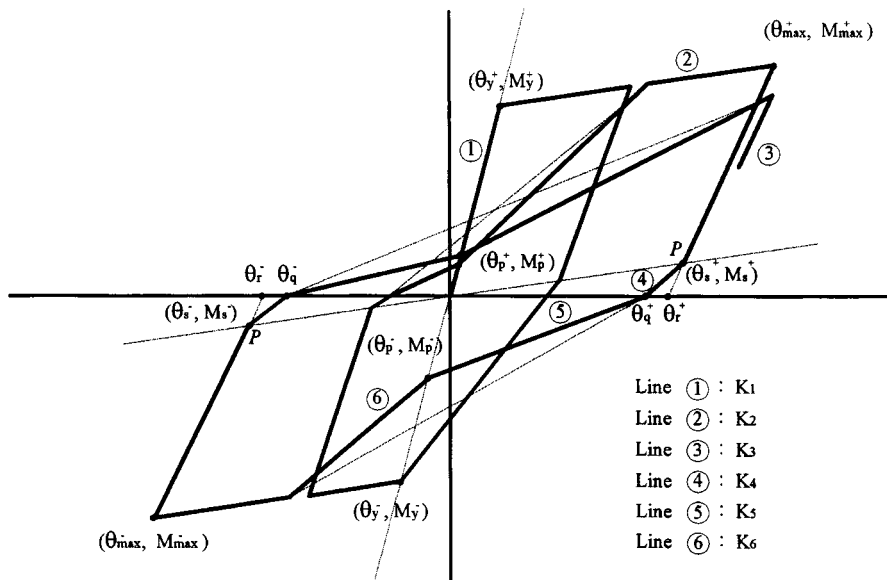

Fig. 3 Basic hysteretic rule

$$\Delta M = K_3 \Delta\Theta = \frac{M_{max}^+}{\Theta_{max}^+ - \Theta_r^+} \Delta\Theta \tag{10}$$

The superscripts "+" and "−" denote loading in the positive and negative direction, respectively.

4) Inelastic Unloading in the Vicinity of Load Reversal: The stiffness of inelastic unloading in the vicinity of load reversal is different from that of general unloading:

$$\Delta M = K_4 \Delta\Theta = \frac{M_s^+}{\Theta_s^- - \Theta_q^+} \Delta\Theta \tag{11}$$

5) Inelastic Reloading during Closing of Cracks: In a reversed load cycle, the "pinching" of the moment-rotation curve can become significant because of the reduced stiffness before crack closure. This effect can be simulated by introducing the "crack-closing moment", M_p, which is a function of the shear force (Chung and Meyer 1989):

$$\Delta M = K_5 \Delta\Theta = \frac{M_p^+}{\Theta_p^+ - \Theta_q^+} \Delta\Theta \tag{12}$$

6) Inelastic Reloading after Closing of Cracks: Once the absolute value of the moment exceeds the crack-closing moment, M_p, and still increases, then the moment-rotation relationship becomes

$$\Delta M = K_6 \Delta\Theta = \frac{M_{max}^+ - M_p^+}{\Theta_{max}^+ - \Theta_p^+} \Delta\Theta \tag{13}$$

3.2. Stiffness degradation during inelastic unloading

If the load is reduced after the yielding of the tensile reinforcement, the flexural stiffness is restored to a value somewhat less than the initial stiffness K_1. This stiffness degradation is generally considered to be a function of ductility ratio δ_{max}/δ_y (Takeda *et al.* 1970), determined either graphically (Chung and Meyer 1989) or analytically (Seo 1990). But Seo's method does not consider the stiffness degradation accompanied by the strength deterioration under constant ductility ratio. Also Chung's graphical method captures the strength degradation phenomenon only incompletely. The flexural stiffness, according to Chung's method, experiences an abrupt change in the vicinity of load reversal, which is not observed in laboratory tests. The stiffness degradation, therefore, is considered here as a function of ductility ratio and yield moment ratio M_{max}/M_y, Fig. 4,

$$K_3 = \left(\frac{1}{\mu}\right)^\alpha \xi K_1 \tag{14}$$

where $\mu = \delta_{max}/\delta_y$, $\xi = M_{max}/M_y$, $\alpha = 0.5$

3.3. Inelastic unloading in the vicinity of load reversal

Seo (1990) assumes that the drastic flexural stiffness reduction in the vicinity of load reversal starts at point P (Fig. 3). From the analysis of test results, however, it is found that the point of steep reduction in stiffness depends on the maximum shear stress in a member. The strain-hardening stiffness K_2 is now replaced by K_2',

$$K_2' = \frac{K_2}{(v_{max}/\sqrt{f_c'})^\gamma} \tag{15}$$

where v_{max} is the maximum shear stress in the member, and $\gamma=2.5$. The stiffness degradation in this region is now defined as a function of the pinching coefficient (Fig. 4),

$$K_4 = K_3 \, \eta \left(\frac{1}{\mu}\right)^\beta \tag{16}$$

where

$$\eta = \begin{array}{ll} 0.5 & \text{if } (a/d) < 1.5 \\ 0.2(a/d) + 0.2 & \text{if } (a/d) \ 1.5 < (a/d) < 4.0 \\ 1.0 & \text{if } (a/d) > 4.0 \end{array}$$

is the pinching coefficient, $\beta = 0.32(v_y/\sqrt{f_c'})^{0.5}$ where v_y is the shear stress at flexural yielding, and (a/d) is the member's shear span ratio.

3.4. Stiffness degradation during inelastic loading

When the load reversal occurs within the inelastic range in the presence of shear stress, the shear force is mostly transferred through dowel action, which provides rather low stiffness. After the closure of such cracks, aggregate interlock and shear friction cause a significant increase of the member stiffness. Roufaiel and Meyer (1983) considered this effect by introducing the crack-closing moment M_p^+. Other researchers enhanced this concept by adding such variables as shear span ratio, maximum shear stress, ductility ratio, and the number of load cycles (Chung and Meyer 1989, Seo 1990). Among the variables considered, the number of load cycles may be difficult to track in a frame analysis. And the amount of pinching is reduced in proportion to the maximum moment of each cycle under constant ductility ratio cycling. Thus the crack-closing moment M_p^+ is determined here as follows (Fig. 5),

$$K_5 = \frac{M_p}{\Theta_p - \Theta_q} \tag{17}$$

where and $M_p = M_n \, \eta \, (1/\mu)^\beta (1/\xi)^{4\beta}$ and $\Theta_p = M_p/K_1$.
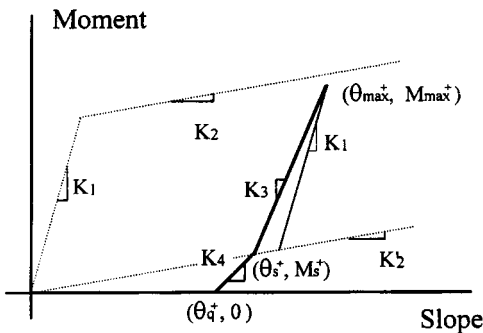

Fig. 4 Stiffness deterioration during inelastic unloading
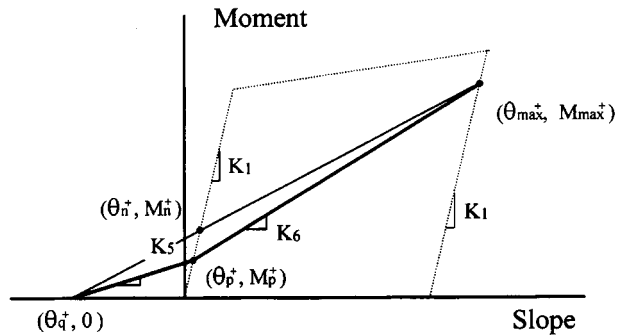
Fig. 5 Stiffness deterioration during inelastic reloading

3.5. Strength deterioration

The strength deterioration of RC members during cyclic loading commences at inelastic reloading, when a previously open crack closes again. The rate of strength deterioration depends on many factors, such as the concrete strength, axial force level, confinement ratio, etc., Chung and Meyer (1989) introduced the imaginary point M_x, towards which the load-deformation curve is aimed during reloading in order to reproduce the strength drop. Herein, Chung's model is modified by replacing the curvature with member slope (see Fig. 6),

$$\Delta M = [(\Theta_f - \Theta_y) K_2 + M_y - M_f] \left(\frac{\Theta - \Theta_y}{\Theta_f - \Theta_y} \right)^w \tag{18}$$

However, the amount of strength reduction given by Eq. (18) is very sensitive to the constant w, which needs to be determined from experimental data. Herein, w is determined as a function of the section aspect ratio (d/b) and the ratio of transverse reinforcement spacing to the beam depth (d/s), which are usually ignored in section analysis, but greatly affect hysteretic behavior.

The ACI 318-89 Code sets a limit on the maximum spacing of transverse reinforcement (d/s=4.0) to ensure ductile beam behavior. Therefore this limiting ratio was selected when determining the constant w,

$$w = 2.1 \left(\frac{(d/s)}{4} \right)^{0.22} \left(\frac{1.5}{(d/b)} \right)^{1.4} \tag{19}$$

where d is the effective depth of a beam, b is the width of a beam and s is the spacing of a transverse reinforcements.

The section aspect ratio (d/b) varies widely in design practice. In Eq. (19), a value of (d/b=1.5) is assumed as the reference value.
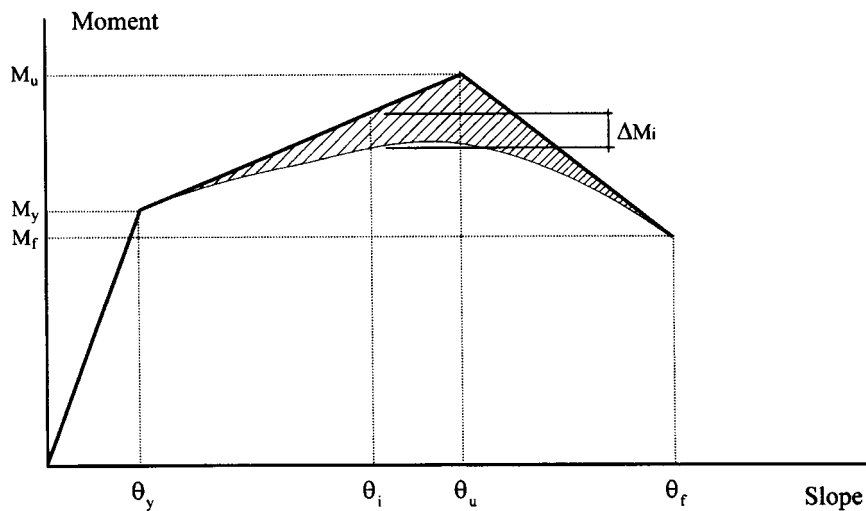

Fig. 6 Strength deterioration curve

Table 1 Specimen list

Researcher	Specimen	a/d^{*1}	$v_m/\sqrt{f_c'}$	w^{*2}	Plastic Hinge
Scribner, Wight	3	4.10	3.06	2.02	Column Face
Scribner, Wight	5	3.60	3.35	2.60	Column Face
Scribner, Wight	7	4.10	3.60	2.28	Column Face
Scribner, Wight	9	5.00	4.92	2.32	Column Face
Scribner, Wight	11	4.00	6.16	2.32	Column Face
Hwang, Scribner	S1-2	4.10	3.60	2.10	Column Face
Hwang, Scribner	S3-2	2.63	7.30	2.10	Column Face
Hwang, Scribner	S3-3	2.63	7.00	2.10	Column Face
Hwang, Scribner	S3-4	2.63	7.40	2.10	Column Face
Nmai, Darwin	F-1	3.90	3.01	1.11	Column Face
Nmai, Darwin	F-2	3.90	3.31	1.11	Column Face
Nmai, Darwin	F-4	3.90	2.14	1.35	Column Face
Nmai, Darwin	F-5	3.90	2.16	1.27	Column Face
Nmai, Darwin	F-7	3.90	2.22	1.30	Column Face
Lee, Kim	C42	4.30	2.61	2.52	Column Face
Lee, Kim	IM42	4.30	2.69	2.54	Moving
Lee, Kim	C25	2.57	5.05	2.94	Column Face
Lee, Kim	IM34	3.14	3.72	2.80	Moving

[*1] Shear span ratio
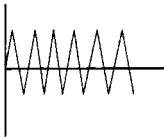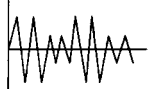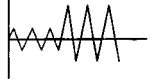[*2] Strength deterioration coefficients, (Formula 19)

Table 2 Loading history

No.	Loading history	Specimen	Researcher
1		3	Scribner, Wight
		5	Scribner, Wight
		7	Scribner, Wight
		9	Scribner, Wight
		22	Scribner, Wight
		F-1	Nmai, Darwin
		F-2	Nmai, Darwin
		F-4	Nmai, Darwin
		F-5	Nmai, Darwin
		F-7	Nmai, Darwin
		S1-2	Hwang, Scribner
		S3-2	Hwang, Scribner
2		S3-3	Hwang, Scribner
3		S3-4	Hwang, Scribner
4		C25	Lee, Kim
		C42	Lee, Kim
		IM34	Lee, Kim
		IM42	Lee, Kim

Table 3 Energy dissipation capacity (Unit: kips in)

	Scribner and Wight					Hwang and Scribner				Nmai and Darwin					Lee and Kim			
	3	5	7	9	11	S1-2	S3-2	S3-3	S3-4	F-1	F-2	F-3	F-5	F-7	C42	IM42	C25	IM34
Analysis	315	253	460	1027	772	376	167	200	173	236	138	216	194	158	705	412	954	554
Test	311	315	407	1269	723	343	155	196	178	287	169	297	262	201	723	435	944	450
Analysis/Test	1.01	0.80	1.13	0.81	1.07	1.10	1.08	1.02	0.97	0.83	0.82	0.73	0.74	0.79	0.98	0.95	1.01	1.23

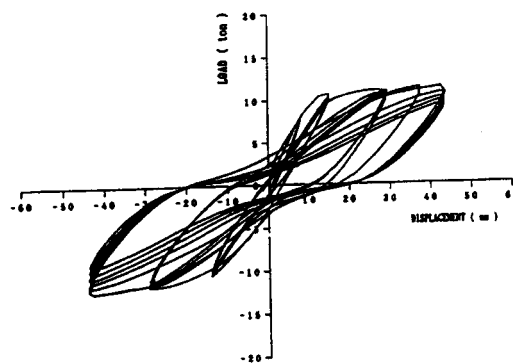# 4. Comparison of test results with analytical results

To verify the proposed analytical model, experimental results of eighteen cantilever specimens tested under displacement control and various loading histories by previous researchers were used:
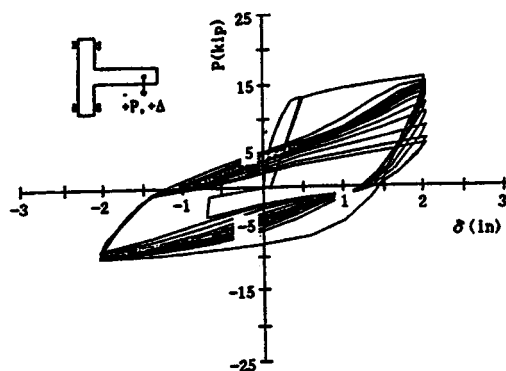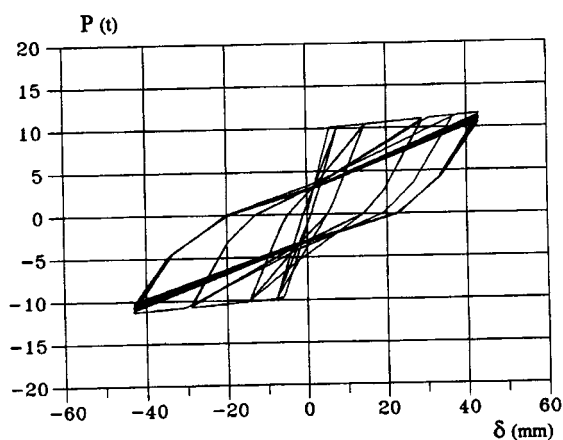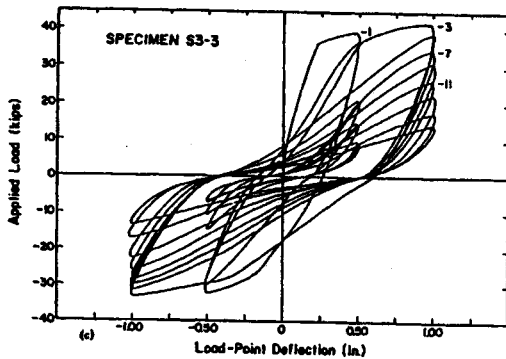

(a) Experiment
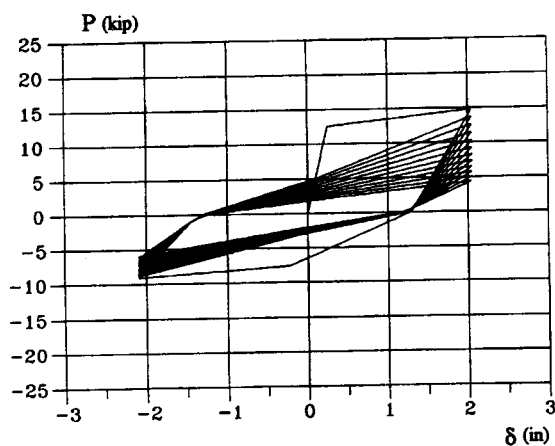
(a) Experiment

(b) Analysis

(b) Analysis

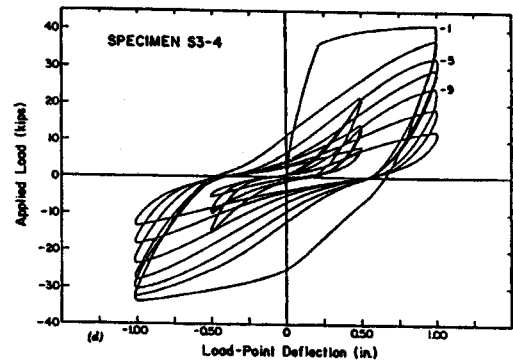Fig. 7 Experimental and analytical load-deflection curve for beam F-4 tested by Nmai and Darwin

Fig. 8 Experimental and analytical load-deflection curve for beam IM-42 tested by Lee and Kim

five specimens tested by Scribner and Wight (1980), four specimens of Hwang and Scribner (1984), five specimens of Nmai and Darwin (1986), and four specimens tested by Lee and Kim (1989). The data used in the analysis of these test specimens are summarized in Table 1, and characteristics of the loading histories are listed in Table 2.

The accuracy of the proposed model can be determined by comparing the energy dissipation capacity of the test beams with the analytical results. The analytical and experimental results agree well, within errors of 27%. Selected representative numerical simulations are reproduced in Figs. 7 to 10 to illustrate the good agreement between the experimental and analytical load-deformation curves. Only for Nmai and Darwin's specimens, analytical results for energy dissipation capacities show relatively large deviations from test results, in spite of good agreement between maximum load levels at each cycle, as seen in the load-deformation curves. The test results exhibit relatively little pinching in the negative direction compared with the positive direction, an unexpected behavior that might warrant further study.
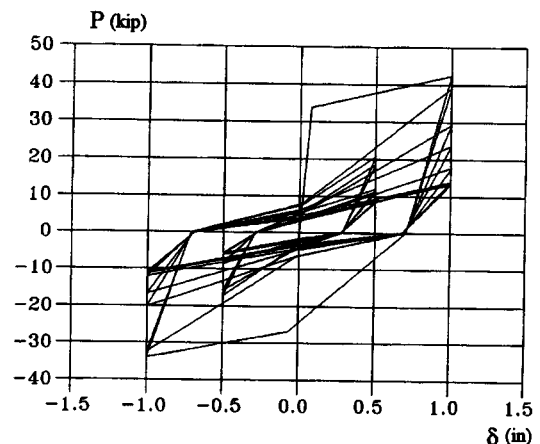
(a) Experiment

(a) Experiment
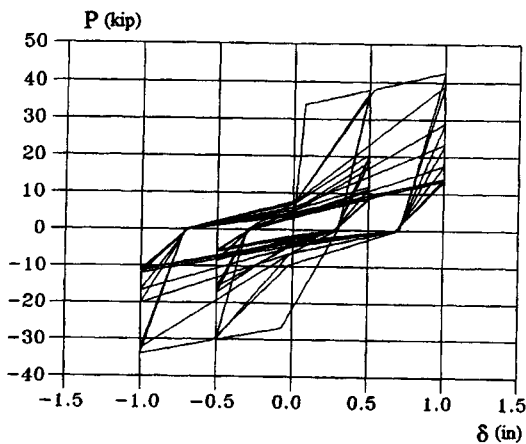
(b) Analysis

(b) Analysis

Fig. 9 Experimental and analytical load-deflection curve for beam S3-3 tested by Hwang and Scribner

Fig. 10 Experimental and analytical load-deflection curve for beam S3-4 tested by Hwang and Scribner

5. Conclusions

The analytical model reported by Chung and Meyer has been modified and improved to simulate the hysteretic behavior of RC beams under various loading histories. The stiffness deterioration caused by inelastic loading is predicted by introducing a function of basic pinching coefficients, ductility ratio (δ_{max}/δ_y), and yield moment ratio (M_{max}/M_y) of members. Also, an improved formulation for the strength degradation coefficient is proposed for capturing the effect of the transverse reinforcement spacing ratio (d/s) and section aspect ratio (d/b) on the inelastic behavior of members.

The accuracy of the proposed model has been verified by comparing analytical results for the energy dissipation capacities with test results obtained by several researchers. Agreement between analytical and test results stayed within errors of 27%.

Acknowledgements

References

Al-Haddad, M.S. and Wight, J.K. (1986), "Feasibility and consequences of moving beam plastic hinging zones for earthquake resistant design of R/C buildings", The University of Michigan, Ann Arbor.

Arzoumanidis, S. and Meyer, C. (1981), "Modeling reinforced concrete beams subjected to cyclic loads", *Technical Report No. NSF-PER-7924695-CU-1*, Columbia University, March.

Brown, R.H. and Jirsa, J.O. (1971), "Reinforced concrete beams under load reversals", *ACI J.*, **68**(5), 380-390.

Chung, Y.S., Meyer, C. and Shinozuka, M. (1989), "Modeling of concrete damage", *ACI Structural Journal*, **86**(3), 259-271.

Giberson, M.F. (1967), "The response of nonlinear multi-story structures subjected to earthquake excitation", Ph.D. Thesis, California Institute of Technology, Pasadena, California.

Giberson, M.F. (1969), "Two nonlinear beams with definition of ductility", *J. Strut. Div., ASCE*, **95**(2), 137-157.

Guan, H. and Loo, Y.C. (1977), "Layered finite element method in cracking and failure analysis of RC beams and beam-column-slab connections", *Structural Engineering and Mechanics*, **5**(5), 645-666

Hwang, T.H. and Scribner, C.F. (1984), "R/C member cyclic responses during various loading", *J. Struct. Eng., ASCE*, **110**(3), 477-489.

Lee, L.H. and Kim, Y.I. (1989), "Shear reinforcement and relocating plastic hinging zones of R/C beams subjected to cyclic load", *Proc., Architectural Institute of Korea*, **18**(2), 627-630.

Ma, S.M., Bertero, V.V. and Popov, E.P. (1976), "Experimental and analytical studies on hysteretic behavior of reinforced concrete rectangular and T-beams", Report No. EERC 76-2, Earthquake Eng. Center, University of California, Berkeley, California.

Mander, J.B., Priestley, M.J. and Park, R. (1988), "Theoretical stress-strain model for confined concrete", *J. Strut. Eng., ASCE*, **114**(8), 1804-1826.

Nmai, C.K. and Darwin, D. (1986), "Lightly reinforced concrete beams under load reversals", *ACI J.*, **83**(9), 777-783.

Noguchi, H. and Kashiwazaki, T. (1997), "Finite element analysis of RC beam-column joints with high-

strength materials", *Structural Engineering and Mechanics,* **5**(5), 625-635

Otani, S. and Sozen, M.A. (1972), "Behavior of multistory reinforced concrete frames during earthquake", Civil Engineering Studies, Structural Research Series No. 392, University of Illinois, Urbana, November.

Otani, S. (1974), "Inelastic analysis of R/C frame structure", *J. Strut. Div., ASCE,* **100**(7), 1433-1449.

Ozcebe, G. and Saatcioglu, M. (1989), "Hysteretic shear model for reinforced concrete members", *J. Strut. Eng., ASCE,* **115**(1), 132-149.

Roufaiel, M.S.L. and Meyer, C. (1987), "Analytical modeling of hysteretic behavior of R/C frames", *J. Strut. Div., ASCE,* **113**(3), 429-443.

Roufaiel, M.S.L. and Meyer, C. (1983), "Analysis of damaged concrete frame for cyclic loads", *Earthquake Eng. and Struct. Dynamic,* **11**(?), 207-228.

Scribner, C.F. and Wight, J.K. (1980), "Strength decay in reinforced concrete beams under load reversals", *J. Strut. Div., ASCE,* **106**(4), 861-875.

Seo, S.Y. (1990), "Analysis of hysteretic behavior of R/C members subjected to load reversals - Single component model having the finite size of plastic regions -", MS Thesis, Department of Architectural Engineering, Han Yang University, Seoul, Korea.

Shiha, B.P., Gerstle, K.H. and Tulin, L.G. (1964), "Stress-strain relationship for concrete under cyclic loading", *ACI J.,* **61**(2), 195-211.

Takeda, T., Sozen, M.A. and Nielson, N.N. (1970), "Reinforced concrete response to simulated earthquakes", *J. Strut. Div., ASCE,* **96**(7), 2557-2573.

Appendix A

1) slope in plastic hinging zone (Fig. 1 (b)).

$$\Theta = \frac{M}{(EI)} x_i$$
$$= M x_i \frac{c(EI)_e + (1-c)(EI)_p}{(EI)_p(EI)_e}$$
$$= M x_i \frac{(EI)_e + (EI)_p}{2[(EI)_p(EI)_e]} \text{ (in case that } c=0.5)$$
$$= \frac{M}{2}\left(\frac{1}{(EI)_p} + \frac{1}{(EI)_e}\right) x_i$$

2) slope in flexural rotational spring (Fig. 1 (c)).

$$\Theta = \frac{(\phi_p + \phi_e)}{2} x_i$$
$$= \left(\frac{M}{(EI)_p} + \frac{M}{(EI)_e}\right)\left(\frac{x_i}{2}\right)$$
$$= \frac{M}{2}\left(\frac{1}{(EI)_p} + \frac{1}{(EI)_e}\right) x_i$$